Optics Communications 285 (2012) 3242–3245

Contents lists available at SciVerse ScienceDirect

Optics Communications

journal homepage: www.elsevier.com/locate/optcom

Nanometeric plasmonic refractive index senor

Jia Hu Zhu, Xu Guang Huang *, Jin Tao, Xiao Ping Jin, Xian Mei

Laboratory of Nanophotonic Functional Materials and Devices, South China Normal University, Guangzhou, 510006, China

ARTICLE INFO

Article history:
Received 17 November 2010
Accepted 24 February 2012
Available online 9 March 2012

Keywords:
SPP
Sensor
Refractive index
Metal–insulator–metal waveguide

ABSTRACT

A novel surface plasmon-polaritons (SPPs) refractive index sensor based on tooth-shaped metal–insulator–metal structure is proposed and numerically simulated by using the finite difference time domain method with perfectly matched layer absorbing boundary condition. Both analytic and simulated results show that the transmission minima wavelengths in the transmitted spectrum of the sensor have a linear relationship with the refractive index of material under sensing. Based on the relationship, the refractive index of the material can be obtained from the detection of one of the transmission minima wavelengths in the transmitted spectrum. The resolution of refractive index of the nanometeric sensor can reach as high as 10^{-6}, given the wavelength resolution of 0.01 nm. It could be applied to high-resolution biological sensing.

1. Introduction

Nowadays, several different metal–insulator–metal (MIM) waveguide structures based on SPP have been numerically and/or experimentally demonstrated, such as U-shaped waveguides [1], splitters [2], Y-shaped combiners [3], multimode-interferometers [4], couplers [5,6] and Mach–Zehnder interferometers [7,8]. The different functions have been realized based on the MIM waveguide structures, such as the splitter [2], the filter [9] and the optical switch [10]. In this paper, we have proposed and demonstrated a nanometeric plasmonic refractive index (RI) senor based on tooth-shaped MIM waveguide structure. In the past decade, a surface plasmon sensor that is a type of evanescent field-based sensors has been widely researched. Today, several integrated optical SPR sensors have been demonstrated [11–13], in which thin metal films were deposited on tops of integrated optical waveguides as platforms for the attachment of sensing films. However, all of those integrated SPR sensors were made in dielectric materials with low RI contrast, thus typical dimensions of waveguides and optical components were too large to be miniaturized, and it is unsuitable for lab-on-chip applications. Compared with other sensors, SPPs sensors have an inherent advantage to achieve high integration.

In this paper, a novel SPPs sensor based on a tooth-shaped MIM waveguide structure is proposed. The finite difference time domain (FDTD) method in a perfectly matched layer (PML) absorbing boundary condition is employed to simulate and research its properties. The relation between the transmission minima wavelengths in the transmission spectrum and the effective index of the material (liquid or gas) under sensing (MUS) is analyzed. It is ultracompact in dimension with a few hundred nanometers for high integration.

2. Devices structure and theoretical analysis

To begin with the dispersion relation of the fundamental TM mode in an MIM waveguide (shown in the inset of Fig. 1) is given by [14,15]

$$\varepsilon_{in}k_{z2} + \varepsilon_m k_{z1}\coth(ik_{z1}\omega/2) = 0, \tag{1}$$

with k_{z1} and k_{z2} defined by momentum conservation

$$k_{z1}^2 = \varepsilon_{in}k_0^2 - \beta^2, \quad k_{z2}^2 = \varepsilon_m k_0^2 - \beta^2, \quad \varepsilon_{in} = n^2. \tag{2}$$

Where ε_{in} is dielectric constant of the insulator, β is the propagation constant and $k_0 = 2\pi/\lambda_0$ is the free-space wave vector. The frequency-dependent complex relative permittivity ε_m of silver is characterized by the Drude–Lorentzian model with its dielectric constant

$$\varepsilon_m(\omega) = \varepsilon_\infty - \frac{\omega_D^2}{\omega^2 + i\gamma_D\omega} - \sum_{m=1}^{2}\frac{g_{Lm}\omega_{Lm}^2\Delta\varepsilon}{\omega^2 - \omega_{Lm}^2 + i2\gamma_{Lm}\omega}. \tag{3}$$

Where $\varepsilon_\infty = 2.3646$, $\omega_D = 8.7377$ eV, $\gamma_D = 0.07489$ eV, $\Delta\varepsilon = 1.1831$, $g_{L1} = 0.26663$, $\omega_{L1} = 4.3802$ eV, $\gamma_{L1} = 0.28$ eV, $g_{L2} = 0.7337$, $\omega_{L2} = 5.183$ eV, and $\gamma_{L2} = 0.5482$ eV give a good description of empirical dielectric constant data for silver [16]. The real part of the propagation constant β is represented as the effective index $n_{eff} = \text{real}(\beta/k_0)$ of the waveguide for SPPs. w is the width of slit (it is fixed to be 50 nm). In the dispersion relation, as a function of the refractive index n of the MUS for different incident wavelengths, n_{eff} of the slit waveguide is calculated and displayed in Fig. 1. Obviously, n_{eff} is almost linear with the refractive index n within the range of 1.0–1.6 at all wavelengths.

It should be noted that the dependence of n_{eff} on the refractive index n of the MUS is also suitable to the small part or region of the tooth waveguide with the tooth width of w_t shown in Fig. 2.

* Corresponding author.
E-mail address: huangxg@scnu.edu.cn (X.G. Huang).

0030-4018/$ – see front matter © 2012 Elsevier B.V. All rights reserved.
doi:10.1016/j.optcom.2012.02.097

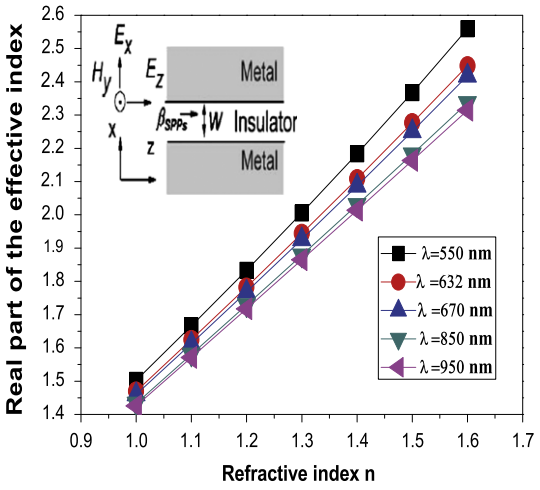

Fig. 1. Real part of the effective index n_{eff} versus the refractive index n of the MUS in a MIM slit waveguide structure for different incident wavelengths of $\lambda = 550$ nm, 632.8 nm, 670 nm, 850 nm, and 950 nm.

The waveguide sensor is shown in Fig. 2. The structure of the device is composed of a slit and a tooth which are filled with the material (liquid or gas) under sensing (MUS). The waveguide can be filled up with gaseous or liquid MUS by different methods. Simply gaseous MUS can be diffused into the waveguide based on gas diffusion force in vacuum circumstance. Liquid MUS can be filled up into the cavity using nano-filling technique based on capillarity attraction [17–19].

In Fig. 2, r_i, t_i, and s_i ($i = 1, 2, 3$) are, respectively, the reflection, transmission, and splitting coefficients of an incident beam from Port i ($i = 1, 2, 3$) caused by the structure; and E_i^{in} and E_i^{out} stand for the fields of incident and output beams at Port i, respectively. For the case of $E_2^{in} = 0$, one has

$$E_2^{out} = t_1 E_1^{in} + s_3 E_3^{in}, \tag{4}$$

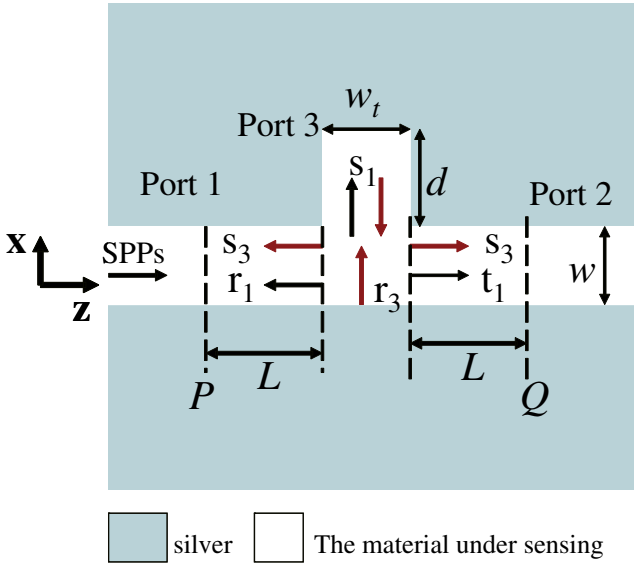

Fig. 2. Schematics of a single tooth-shaped waveguide structure with a slit width of w, a tooth width of w_t, and a tooth depth of d.

in which E_3^{in} is given as follows:

$$\begin{aligned} E_3^{in} &= s_1 E_1^{in} \exp(i\varphi(\lambda))\left(1 + r_3 \exp(i\varphi(\lambda)) + r_3^2 \exp(i\varphi(\lambda)) + \ldots\right) \\ &= \frac{s_1 E_1^{in}}{1 - r_3 \exp(i\varphi(\lambda))} \exp(i\varphi(\lambda)), \end{aligned} \tag{5}$$

where the phase delay $\phi(\lambda) = (4\pi/\lambda).n_{eff}.d + \Delta\varphi(\lambda)$ and $\Delta\phi(\lambda)$ is the phase shift caused by the reflection on the air–silver surface. Combining Eqs. (4) and (5), the output field at Port 2 is derived as

$$E_2^{out} = t_1 E_1^{in} + \frac{s_1 s_3 E_1^{in}}{1 - r_3 \exp(i\varphi(\lambda))} \exp(i\varphi(\lambda)) \tag{6}$$

Therefore, the transmittance T from Port 1 to Port 2 is given by

$$T = \left|\frac{E_2^{out}}{E_1^{in}}\right|^2 = \left|t_1 + \frac{s_1 s_3}{1 - r_3 \exp(i\varphi(\lambda))} \exp(i\varphi(\lambda))\right|^2. \tag{7}$$

It can be seen from Eq. (7) that, if the phase satisfies $\phi(\lambda) = (2m+1)\pi$ ($m = 0, 1, 2\ldots$), the two terms inside the absolute value sign on the right of the equation will cancel each other. Therefore, the transmission minima wavelength λ_m is determined as follows:

$$\lambda_m = \frac{4 n_{eff} d}{(2m+1) - \Delta\varphi(\lambda)/\pi}, (m = 0, 1, 2\ldots). \tag{8}$$

It can be seen that the wavelength λ_m is linear with the effective index n_{eff}. In the following FDTD simulations, the order of m is equal to 0. And from Fig. 1, n_{eff} is almost linear with the refractive index n at all wavelengths. Therefore the wavelength λ_m is linear with the RI. And the RI of the MUS can be obtained from the measurement of the wavelength λ_m.

A calibration should be required for precise sensing, before the measurement of the refractive index of an unknown material. It could be operated as follows. The sensor is respectively filled up with different materials whose refractive indices are known, and the dip wavelength of the transmission spectrum is detected orderly. The cleaning of the sensor is required before every measurement. A calibration curve can be obtained as the transmission minima wavelength versus the refractive index.

3. Simulation experiment and results

In the following FDTD simulations, the grid sizes in the x and the z directions are chosen to be 5 nm × 5 nm. The fundamental TM mode of the plasmonic waveguide is launched at the beginning of the structure. Two power monitors are, respectively, set at the points of P and Q to detect the incident and the transmission fields for calculating the incident power of P_{in} and the transmitted power of P_{out}. The transmittance is defined to be $T = P_{out}/P_{in}$.

Fig. 3(a) shows a typical transmission spectrum of the structure with $w_t = 50$ nm, $w = 50$ nm, and $d = 100$ nm. In Fig. 3(a), it is can be seen that the transmission minima occur at the wavelength of 775 nm with the transmittance of −33 dB. Fig. 3(b) shows that the transmission minima wavelength shifts linearly toward longer wavelength when the tooth depth d is increased and other parameters are fixed. From Eq. (8) one can see that the relationship between the transmission minima wavelength and the tooth depth is a linear function for given w and w_t.

Fig. 4 shows the transmission spectra of the sensor for different refractive indices with the same $w = 50$ nm, $w_t = 50$ nm, and $d = 100$ nm. The FDTD simulation results reveal that the transmission minima wavelength shifts toward long wavelength with the increasing of refractive index of the sensor.

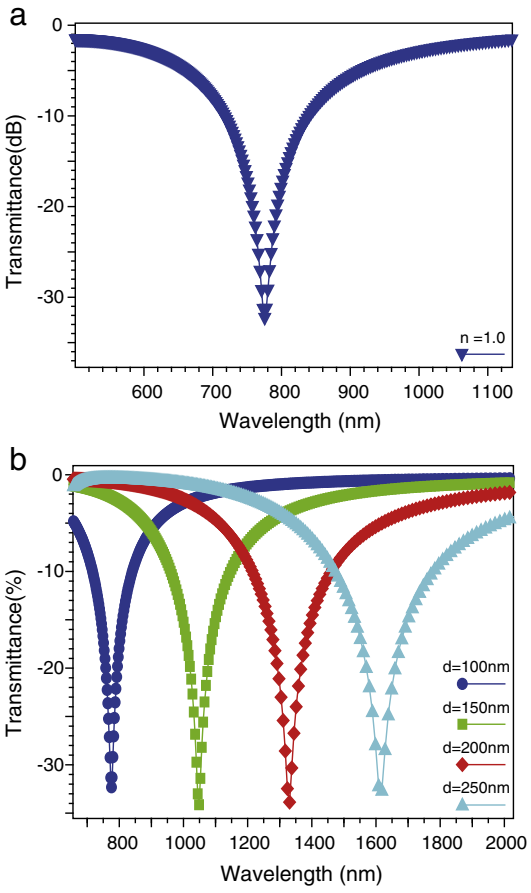

Fig. 3. (a) Transmission spectrum of the sensor structure with $w=50$ nm, $w_t=50$ nm, $d=100$ nm. (b) The transmission spectra at various tooth depths of d increasing with the same $w=50$ nm, $w_t=50$ nm.

Fig. 5 shows that the relationship between the transmission minima wavelength and the refractive index of the MUS is a linear function with the RI dispersion of $dn/d\lambda=1.37\times10^{-3}$ nm^{-1} for given w and d. The FDTD simulation result is very similar to the theoretical analysis above. Obviously, one can obtain the refractive index n of the MUS from detecting the transmission minima wavelength λ_m. Nowadays, a high-resolution optical spectrum analyzer can achieve a wavelength resolution of $\Delta\lambda=0.01$ nm. The sensing resolution of the refractive index is defined as $SR=(dn/d\lambda)\times\Delta\lambda$. With the RI dispersion in Fig. 5 and the wavelength resolution, the sensing resolution of the refractive index can be achieved to be $SR=1.37\times10^{-5}$.

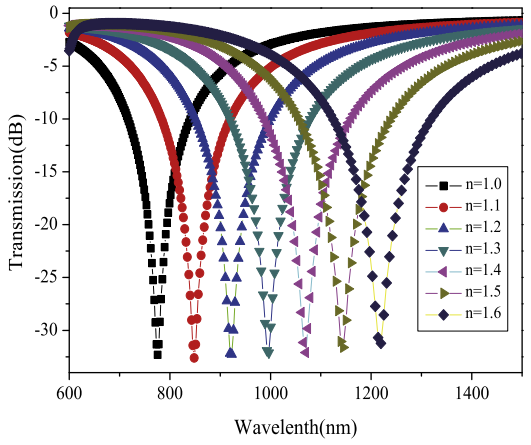

Fig. 4. The transmission spectra of the sensor for different refractive indices with the same $w=50$ nm, $w_t=50$ nm, and $d=100$ nm.

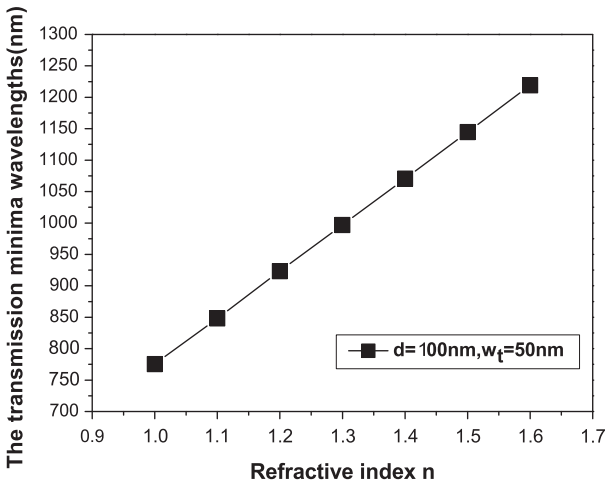

Fig. 5. The transmission minima wavelength versus the refractive index n of the MUS.

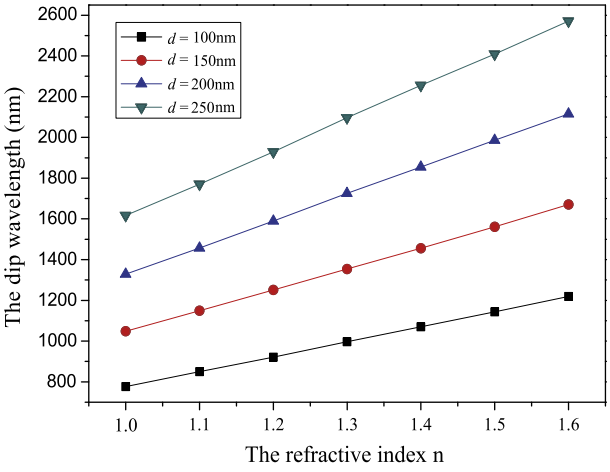

Fig. 6. The transmission minima wavelength versus the refractive index of the MUS with different tooth depths and a given tooth width of $w=50$ nm.

Fig. 6 shows that the transmission minima wavelength of the sensor as a function of the refractive index with different tooth depths. One can see that the larger the tooth depth is, the higher the resolution SR of the sensor. Thus the resolution SR can be enhanced by increasing the tooth depth. The resolution SR approaches 6.24×10^{-6}, when the tooth depth is 250 nm.

4. Conclusion

In conclusion, a novel SPPs RI sensor based on a tooth-shaped MIM waveguide is reported. The simulation demonstrates that the resolution SR of the RI sensor can achieve the order of magnitude of 10^{-6}, assuming a wavelength resolution of 0.01 nm. The RI sensor could be applied to high-resolution biologic sensing because of its high resolution.

Acknowledgments

The authors acknowledge the financial support from the National Natural Science Foundation of China (Grant no. 61077038) and the Natural Science Foundation of Guangdong Province, China (Grant no. 07117866).

References

[1] T.W. Lee, S. Gray, Optics Express 13 (24) (2005) 9652.
[2] G. Veronis, S. Fan, Applied Physics Letters 87 (13) (2005) 131102.
[3] H. Gao, H. Shi, C. Wang, C. Du, X. Luo, Q. Deng, Y. Lv, X. Lin, H. Yao, Optics Express 13 (26) (2005) 10795.
[4] Z. Han, S. He, Optics Communication 278 (1) (2007) 199.
[5] T. Nikolajsen, K. Leosson, S.I. Bozhevolnyia, Applied Physics Letters 85 (24) (2004) 5833.
[6] H. Zhao, X. Guang, J. Huang, Physica E: Low-dimensional Systems and Nanostructures 40 (10) (2008) 3025.
[7] B. Wang, G.P. Wang, Optics Letters 29 (17) (2004) 1992.
[8] Z. Han, L. Liu, E. Forsberg, Optics Communication 259 (2) (2006) 690.
[9] Q. Zhang, X.G. Huang, X.S. Lin, J. Tao, X.P. Jin, Optics Express 17 (9) (2009) 7549.
[10] C.J. Min, G. Veronis, Optics Express 17 (13) (2009) 10757.
[11] J. Ctyrocky, Sensors and Actuators B 54 (1999) 66.
[12] R.D. Harris, J.S. Wilkinson, Sensors and Actuators B 29 (1995) 261.
[13] J. Homola, J. Ctyrocky, M. Skalsky, J. Hradilova, P. Kolarova, Sensors and Actuators B 38–39 (1997) 286.
[14] A. Boltasseve, S.I. Bozhevolnyi, T. Nikolajsen, K. Leosson, Journal of Lightwave Technology 24 (2006) 912.
[15] J.A. Dionne, L.A. Sweatlock, H.A. Atwater, Physical Review B 73 (2006) 035407.
[16] P.B. Johnson, R.W. Christy, Physical Review B 6 (1972) 4370.
[17] A.Y. Vorobyev, Chunlei Guo, Applied Physics Letters 224102 (1–3) (2009).
[18] D. Ugarte, T. Stockli, J.M. Bonard, A. Chatelain, W.A. de Heer, Applied Physics A: Materials Science and Processing 67 (1998) 101.
[19] D. Ugarte, A. Chatelain, W.A. de Heer, Science 274 (1996) 1897.